Spectroscopic Equipment for the Space Telescope [and Discussion]

D. S. Leckrone and J. P. Connerade

Spectroscopic equipment for the Space Telescope

By D. S. Leckrone

Laboratory for Astronomy and Solar Physics, Goddard Space Flight Center,
Greenbelt, Maryland 20771, *U.S.A.*

The Space Telescope will provide views of the Universe of remarkable clarity. Central to its capabilities is an $f/24$ Ritchey–Chretien telescope with a $40\,000$ cm² unobscured collecting area, which will provide point-source images less than 0.1″ in radius at wavelengths below 633 nm. It will operate over the range 110 nm to 1 mm. The initial flight instrumentation includes two spectrographs, the Faint Object Spectrograph (F.O.S.) and the High-Resolution Spectrograph (H.R.S.). The F.O.S. is sensitive from 115 to 800 nm. It will provide data at resolving powers 10^3–10^2 on extremely faint sources. The H.R.S. operates at the wavelengths 107–320 nm. It will achieve high photometric accuracy at resolving powers 10^5, in the échelle mode, or 10^4–10^3 in first order, on brighter targets. The two cameras on board the S.T. will provide ancillary spectroscopic capabilities.

1. The Space Telescope observatory

With the launch of the Space Telescope (S.T.) by the National Aeronautics and Space Administration in 1985, a decades-old aspiration of astronomers will be fulfilled, namely to be able to observe the Universe with a telescope of large aperture and high optical quality, free from the turbulence, the selective absorption and the brightness of the Earth's atmosphere. The telescope at the heart of the observatory is a 2.4 m Ritchey–Chretien cassegrain configuration with a focal ratio $f/24$. Its unobscured collecting area, $40\,000$ cm², places it in the class of the larger telescopes at mountain-top observatories. The optical quality of the primary and secondary telescope mirrors are believed to be the finest ever achieved for large optics. The full-aperture wavefront error of the primary mirror is at least as good as $\lambda/65$ r.m.s. at 6300 Å†. The goal for overall observatory performance is $\lambda/20$ r.m.s. at 6300 Å. At present it appears likely that the goal will be met. Such performance corresponds to an angular resolution of at most 0.1″ defined in terms of the radius for 70 % encircled energy, at wavelengths ranging from 6300 Å down to 3000 Å or less. The combination of large collecting area and high angular resolution, with the associated rejection of sky background, will allow the S.T. to achieve useful signal:noise ratios in reasonable exposure times on very faint sources. The gain in direct imaging with respect to ground-based telescopes is estimated to be about four magnitudes. The image quality of the S.T. will also allow the resolution and isolation of fine spatial details in extended sources such as galaxies, nebulae, star clusters and planetary disks. The absence of atmospheric 'seeing' and differential refraction will result in photometrically stable and symmetrical images that can be delimited by small and symmetrical apertures. The S.T.'s bandpass encompasses four decades in wavelength, from 1100 Å to 1 mm. However, initially it will not be instrumented for work in the infrared.

† 1 Å $= 10^{-10}$ m $= 10^{-1}$ nm.

[83]

The initial complement of S.T. scientific instruments provides a diversified menu of spectroscopic capabilities, exploiting the characteristics of the observatory described above. Two of the five instruments are dedicated spectrographs. Also, the two S.T. cameras incorporate ancillary spectroscopic modes, which make use of their field-imaging capabilities. These instruments are listed in table 1 and are described in subsequent sections. The Wide Field and Planetary Camera is the only instrument with access to the central area of the S.T. focal surface. The two spectrographs and the Faint Object Camera operate off-axis and must therefore cope with minor amounts of astigmatism and field curvature.

The telescope and the scientific instruments are currently at an advanced stage of flight hardware construction. They are to be delivered so that integration of the overall observatory can begin late in 1983. The design of the spacecraft is essentially complete and its manufacture is under way. Additional information about the S.T. and its instruments may be found in Bahcall & O'Dell (1980) and Leckrone (1980).

TABLE 1. SPECTROSCOPIC EQUIPMENT ON THE SPACE TELESCOPE

instrument	investigator	capabilities
Faint Object Spectrograph	R. J. Harms, University of California, San Diego	moderate and low spectral resolution u.v.–optical spectroscopy u.v. spectropolarimetry time-resolved spectroscopy multiple-aperture-limited spatial resolution
High-Resolution Spectrograph	J. C. Brandt, Goddard Space Flight Center	moderate to very high spectral resolution u.v. spectroscopy solar-blind capability exploratory deep-u.v. spectroscopy time-resolved spectroscopy aperture-limited spatial resolution
Faint Object Camera	European Space Agency	moderate spectral resolution u.v.–optical spectroscopy with simultaneous spatial resolution along slit low spectral resolution u.v.–optical 'objective prism' spectroscopy
Wide Field and Planetary Camera	J. A. Westphal, California Institute of Technology	low spectral resolution u.v. to near-i.r. 'objective grism' spectroscopy

2. THE FAINT OBJECT SPECTROGRAPH

The Faint Object Spectrograph (F.O.S.) is intended to achieve astrophysically useful signal : noise ratios on very faint sources at moderate to low spectral resolving powers. Thus, a premium has been placed on high throughput at ultraviolet and visible wavelengths, on high detector quantum efficiencies, and on low internal noise in its design. Emphasis has also been given to the capability of the F.O.S. to isolate fine angular structure in a variety of source geometries. This has led to the provision of twelve selectable entrance apertures and to packaging of the optical train so that these apertures are located as closely as possible to the telescope's optical axis. The requirement for photometric accuracy has resulted in the selection of detectors that are linear over a wide dynamic range and in the design of mechanisms to be repeatable and structures to be stable within tight tolerances. Finally, the F.O.S. has been designed for scientific versatility, including provisions for ultraviolet spectropolarimetric measurements and for the time-resolution down to 10 ms of spectroscopic observations of rapidly varying sources.

The functional design of the F.O.S., illustrated in figure 1, is notable for its simplicity and compact geometry. The observer may select, by orientation of the spacecraft, either of two independent optical channels, each of which focuses nearly stigmatic spectral images on the photocathodes of photon-counting Digicon detectors. These channels differ only in the wavelength sensitivity of their respective detectors. Light gathered by the telescope comes to a focus at the aperture wheel, containing single or paired apertures ranging in size from 0.1″ to 4.3″ projected on the sky. From there the optical beam may be passed through a polarization analyser, or this device may be rotated out of the beam. The polarization analyser consists of a waveplate, which is rotated in steps of 22.5°, and a Wollaston prism. The deflexion mirror, a
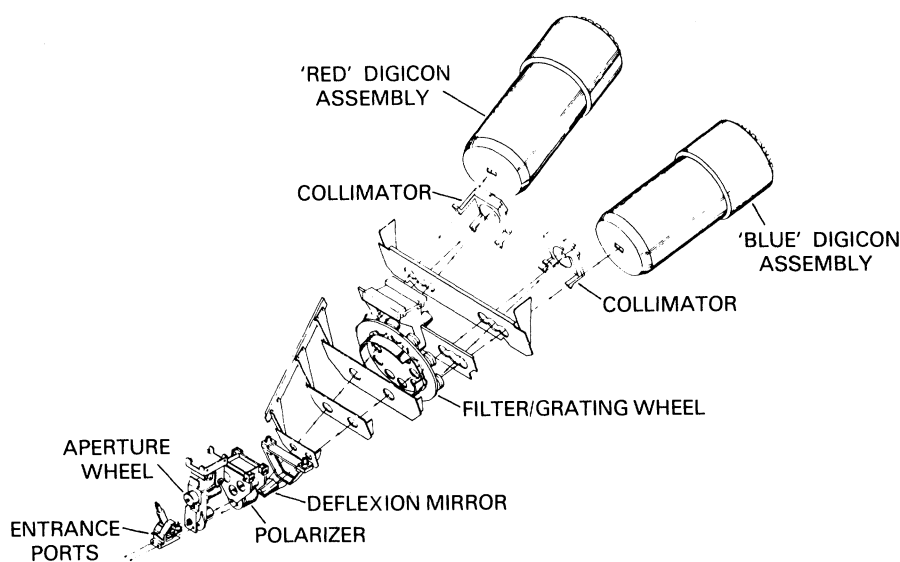

FIGURE 1. Optical design concept for the Faint Object Spectrograph.

'roof' prism, then deflects the beam 22° upward. This simple design feature has the important effect of allowing the apertures to be placed within 61 mm of the telescope's optical axis, physically close to a corner of the instrument, to minimize astigmatism, while also allowing the bulkier components of the spectrograph to be packaged. The deflected beam passes through an order-sorting filter, if required, in the filter/grating wheel. It is collimated by an off-axis paraboloidal mirror and then it is dispersed and focused by the selected element on the filter/grating wheel.

The F.O.S. operates at either of two dispersions, moderate ($R \equiv \lambda/\Delta\lambda = 1230 \pm 185$) or low ($R = 185 \pm 165$). For moderate dispersion observations the dispersing elements are concave gratings that focus first-order spectra on the detector photocathodes. In this mode the wavelength range 1150–8500 Å is divided into six overlapping intervals, covered by six suitably blazed gratings with ruling frequencies ranging from 168 to 954 mm^{-1}. Resolution elements vary in width from 1.1 Å in the far ultraviolet to 6.0 Å at red wavelengths. In low dispersion, concave gratings, with ruling frequencies 144 and 40 mm^{-1}, are used for wavelength intervals 1150–2200 Å and 4000–8000 Å respectively. The corresponding resolution elements are 6.9 and 25 Å. At intermediate wavelengths, 2600–7000 Å, low-dispersion spectra are obtained with the combination of a double-pass, small-angle prism and a concave mirror, mounted in the filter/

grating wheel. The nonlinear dispersion of this element results in resolution varying from 7.4 Å in the ultraviolet to 350 Å in the red. In return for the loss of spectral resolution, the low-dispersion prism provides excellent throughput and image quality. It will doubtless be used for spectrophotometry of the very faintest sources observed with the F.O.S.

The two Digicon detector assemblies, designated 'red' and 'blue', differ only in their photo-cathode and faceplate materials. The 'blue' detector has a bialkali photocathode (Na_2KSb), which is most sensitive at blue and ultraviolet wavelengths, deposited on a magnesium fluoride window. The photocathode of the 'red' detector, trialkali $Na_2KSb(Cs)$ deposited on fused silica, provides an extension of sensitivity to the red, but at the expense of relatively high thermionic noise at ambient temperatures. To reduce dark background to the extremely low
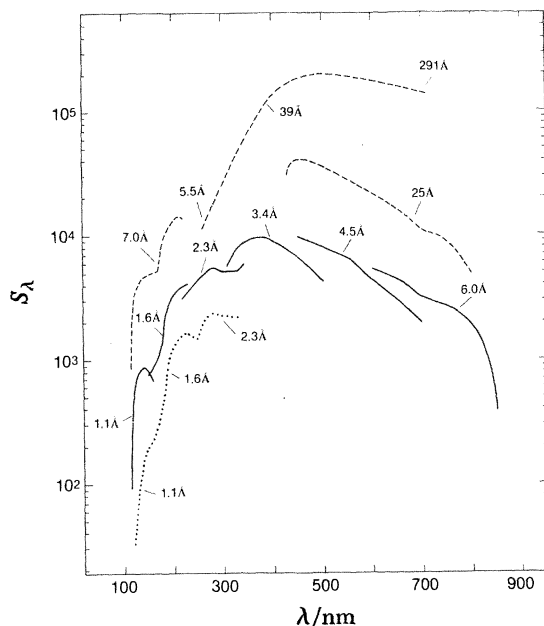

FIGURE 2. Composite sensitivity curves for the Space Telescope and Faint Object Spectrograph. Broken curves represent the low-resolution spectroscopic mode, $R \approx 200$; solid curves represent the moderate-resolution spectroscopic mode, $R \approx 1200$; moderate-resolution spectropolarimetry is denoted by a dotted curve. A 0.25″ entrance aperture is assumed. Each curve is labelled with the corresponding width of a resolution element. S_λ is the ratio of the count per diode per second to the number of photons incident per square centimetre per second per ångström.

values required for the F.O.S.'s scientific programme (a count of less than 0.002 per diode per second), both photocathodes are cooled to the temperature range -10 to -28 °C. The Digicon detector assemblies operate by focusing photoelectrons emitted by the photocathode and accelerated through a potential difference of *ca.* 23 keV, onto a linear array of 512 silicon diodes. Focusing is accomplished with a SmCo permanent magnet assembly, carefully shaped to provide extremely uniform fields. The electron beam can be deflected parallel or perpendicular to the diode array, so that images from any part of the cathode may be centred on the linear array. This facilitates the comparison of sky background and source spectrum or the measurement of both ordinary and extraordinary spectral images in polarimetric observations. The size of each diode, 40 μm × 200 μm, is the optimum to minimize dark noise, but still large enough to prevent a significant loss of signal at the diode ends. The charge pulse generated in each

diode is amplified and counted by one of 512 independent electronic chains. Additional details about Digicon detectors are given in §3.

Substantial progress has already been made in the development of the F.O.S. and in the attainment of its scientific performance objectives. Essentially all flight components have been fabricated and tested. Assembly of the instrument has begun. Two accomplishments of the F.O.S. team deserve special comment. Efficiency measurements of the flight concave gratings for the moderate dispersion mode indicate that values as high as 60% have been achieved in the ultraviolet and as high as 75% at red wavelengths. This represents the best performance of which we are aware for such gratings and will contribute significantly to the objectives of high
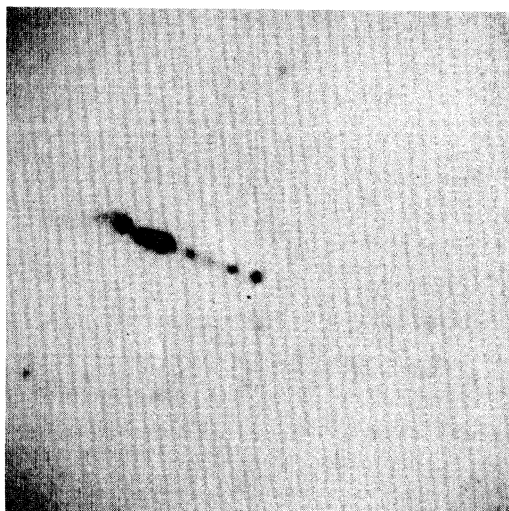

FIGURE 3. Image of the radio galaxy M87, processed to highlight the nucleus and jet. Photo courtesy of J. A. Westphal, California Institute of Technology.

system throughput and faint limiting magnitude. The flight Digicon detectors are also excellent. Measured peak quantum efficiencies are 20% for the bialkali photocathode and 25% for the trialkali, both maxima occurring in the range 2300–2800 Å. The 'blue' tube maintains efficiencies of more than 14% to the MgF_2 cutoff wavelength at 1150 Å. The 'red' tube achieves the goal of extended long-wavelength response. Its measured quantum efficiency at 8000 Å is 2.7%. The goal of very low dark noise in the detectors has also been achieved. A least-squares fit to measured dark count plotted against temperature in the noisier 'red' flight detector indicates a count of *ca.* 0.0013 per diode per second at -10 °C, the warmest expected operational temperature. Under most circumstances in orbit the signal:noise ratio of the F.O.S. will be totally dominated by photon statistics. The dynamic range of the F.O.S. detectors is *ca.* 5×10^7.

With test data available for most flight components of the F.O.S., it is now possible to estimate with some realism the sensitivity of the combined telescope and instrument system. This is illustrated in figure 2 in a form that can be used to estimate the signal one would measure for a given photon flux. All curves shown are based on laboratory measurements except that for the low-dispersion thin prism, for which an estimate based on prior experience is given.

The F.O.S. will provide new insights into the properties of quasars, the nebulosity and jets associated with quasars, the cataclysmic events occurring in the nuclei of active galaxies, and

the possible relation between these events and the quasar phenomenon. It will provide fundamental data about the content, dynamics and evolution of galaxies. It will be used to help establish a more accurate distance scale for the Universe. Data obtained with the F.O.S. will elucidate the properties of rapidly varying X-ray binary systems, pulsars, and strongly magnetic white dwarfs. Because its sensitivity extends to the very faint magnitudes routinely observable with the S.T. cameras, the F.O.S. will provide basic astrophysical information about objects first observed with those cameras.

To illustrate the F.O.S.'s capabilities, we consider the relatively straightforward problem of observing the individual knots, apparently emitters of synchrotron radiation, observed in the jet of the radio galaxy M87. These are illustrated in figure 3, which has been processed to remove the light of the surrounding giant elliptical galaxy, leaving only the image of the galactic nucleus and jet. Eleven knots of diameter less than $0.3''$ have been detected from the ground. They range in brightness from $B = 17$ to $B = 21$ magnitudes. The brightest knots have been observed collectively, with poor spatial and spectral resolution and low sensitivity, with the *International Ultraviolet Explorer* (*IUE*). With the F.O.S. one would like to isolate individual knots in a small aperture (i.e. $0.25''$), to measure the continuous energy distribution and polarization at ultraviolet wavelengths, and to search for line emission. Adopting published ground-based photometry of the individual knots in M87 and extrapolating to the ultraviolet with a power law, $f_\lambda \propto \lambda^{-0.3}$, we estimate fluxes for the knots ranging from 8.3×10^{-6} to 3.9×10^{-4} photons cm^{-2} s^{-1} Å^{-1} at 2000 Å. From figure 2, we determine that the F.O.S. would achieve signal : noise ratios ranging from 16 to 117 in 3 h at moderate dispersion or ranging from 34 to 235 at low dispersion on individual knots at this wavelength. Spectropolarimetry of the brightest knot at the 1% level at moderate dispersion would require an integration time of 5.8 h. At low dispersion, 1% polarimetry would require only 1.4 h on the brightest knot. Thus the F.O.S. will obtain precise astrophysical data, with excellent spatial resolution and useful spectral resolution, on objects that can only be vaguely discerned by the most efficient space instrument currently available.

Additional information about the Faint Object Spectrograph may be found in Harms *et al.* (1979, 1982) and Allen & Angel (1982).

3. The High-Resolution Spectrograph

The design of the High-Resolution Spectrograph (H.R.S.) emphasizes the achievement of higher spectral resolution with greater photometric accuracy than has previously been possible in space ultraviolet astronomical spectroscopy. At spectral resolution $R \approx 2 \times 10^4$, the combined H.R.S. and 2.4 m telescope will reach considerably fainter objects than their predecessors, the *Copernicus* and *IUE* instruments, at comparable resolution. At its highest resolution, $R \approx 10^5$, the H.R.S. has no precedent in extrasolar space astronomy, but is comparable with the large coudé spectrographs at major mountain-top observatories. The latter, in some cases, have optical paths as long as 10 m. Thus the challenge in designing the H.R.S. was to provide a selection of spectral resolutions, including very high R values, covering a broad ultraviolet wavelength interval, within the limited volume allowed for an S.T. instrument, *ca.* 1.8 m^3. Tight constraints were also placed on the design by the requirement that the H.R.S. should accurately measure spectral features as weak as 1% of the neighbouring continuum and that the accuracy of its wavelength measurements should exceed 0.4 resolution elements, i.e. *ca.*

0.005 Å near Ly α at the highest resolution. The former requirement necessitates a system with wide dynamic range, low noise, and excellent electro-optical image quality and uniformity over the field of view. The latter necessitates stable and repeatable positioning of the spectrograph's gratings, reliable onboard spectral calibration sources and a capability of correcting for Doppler shifts introduced by the spacecraft's motion while an observation is proceeding. The various modes in which the H.R.S. will operate are summarized in table 2.

Figure 4 illustrates the H.R.S. design. The observer may select either of two entrance apertures, 0.25″ or 2.0″, by commanded motion of the spacecraft. The apertures are situated approximately 90 mm from the telescope axis. Telescope astigmatism at this point is compensated for by placing separate tangential and sagittal slits at the corresponding foci (1.2 mm separation) and by the off-axis paraboloidal figure of the collimating mirror. At its highest

TABLE 2. OPERATIONAL MODES OF THE H.R.S.

| mode	wavelength range/nm	spectral order	ruling frequency mm^{-1}	$10^{-4} \times$ spectral resolution	detector	spectrum width on detector/nm
1	110–210	1	4960	1.85–2.5	CsTe–MgF$_2$	3.4
2	160–240	1	4320	1.85–2.5	CsTe–MgF$_2$	3.8
3	220–320	1	3600	1.85–2.8	CsTe–MgF$_2$	4.5
4	105–170	1	6000	1.45–2.5	CsI–LiF	2.9
5	105–170	1	600	0.2–0.3	CsI–LiF	29
6	110–170	51–33	316	9.0–10.2	CsI–LiF	0.6–0.9
7	170–320	33–18	316	8.7–11.2	CsTe–MgF$_2$	0.9–1.6
8	115–320	camera	—	—	CsTe–MgF$_2$	215
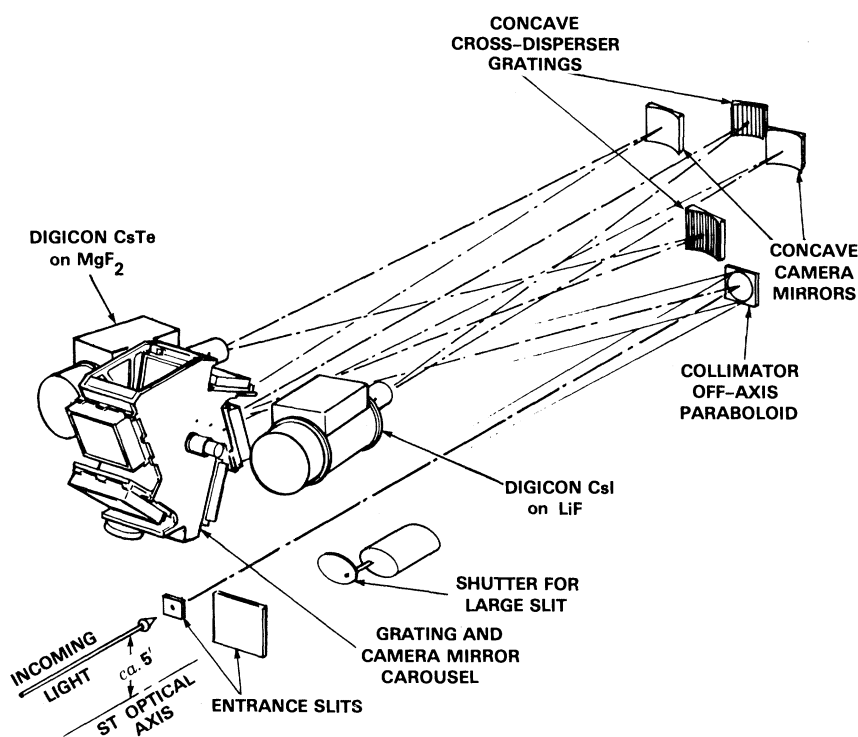
FIGURE 4. Optical design concept for the High-Resolution Spectrograph.

spectral resolution, the instrument is an échelle spectrograph operating in orders 18 to 51. At lower dispersions it operates in first order. Selection of the desired dispersion and detector is accomplished simply by rotation of the grating carousel. The plane échelle and first-order gratings are oriented in their mountings so as to relay the dispersed beam to either of two concave camera mirrors, for first order, or to either of two concave cross-dispersers, for échelle observations, depending on the rotation angle of the carousel. The camera mirrors and cross-dispersers are off-axis paraboloids that produce stigmatic spectral images at the centres of the detector photocathodes. Some residual coma and astigmatism occurs away from the centres. Each photocathode is tilted to optimize image quality in the direction of échelle dispersion. Minor defocusing minimizes the effects of image curvature. Neither of these steps affects the image quality of the first-order spectra. The échelle spectral format, projected on a photocathode plane, consists of 16 or 19 orders of total height *ca.* 17 mm (cross-dispersion) and of maximum width *ca.* 277 mm. The active photocathode area has dimensions 22 mm × 28 mm. Thus only a small wavelength segment can be measured at one time. The desired order is
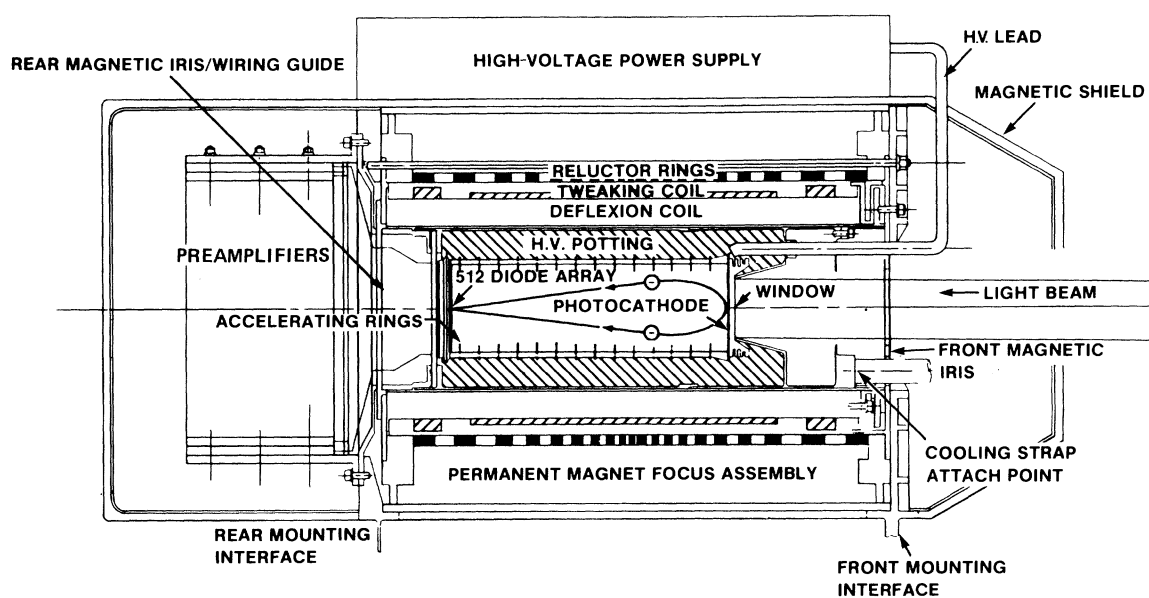

FIGURE 5. Cross section of an H.R.S. Digicon detector assembly. Similar detectors are used in the F.O.S.

centred on the diode array of a Digicon by electromagnetic deflexion of the electron beam emitted by the photocathode. The desired wavelength interval within that order is selected by stepping the grating carousel. Similarly, the desired wavelength interval within a first-order spectrum, of maximum width *ca.* 780 mm, is selected by orientation of the carousel. The detectors' deflexion coils can also move the image along the diode array to allow full sampling of the image spread function, to minimize photometric errors due to variations in sensitivity between diodes and to allow periodic corrections of Doppler shifts due to the spacecraft's orbital velocity.

The H.R.S. incorporates two photon-counting Digicon detectors, which differ only in their photocathode and window materials. A $CsTe-MgF_2$ combination is used to cover the wavelength range 1100–3200 Å. Wavelengths from 1050 to 1700 Å can also be observed with a CsI–LiF combination. The latter is 'solar blind', making it useful for the spectroscopy of cool

stars and planets where one is measuring faint far-ultraviolet fluxes in the presence of a bright, scattered long-wavelength background. Extension of the sensitivity of the CsI–LiF detector to 1050 Å will allow the very weak throughput of the telescope below 1150 Å to be used to observe relatively bright stars in this important wavelength region. A cross-sectional view of an H.R.S. detector assembly is shown in figure 5. The basic functions of the Digicons are summarized in §2. Each of the diodes in the 512-element linear arrays is 400 μm in height to prevent significant loss of signal in the presence of S-distortion and image aberrations, particularly near the corners of the two-dimensional échelle format. The H.R.S. photocathodes are operated at temperatures of *ca.* +20 °C, since neither produces significant thermionic noise. Tests of the flight detector assemblies yield an average background count of less than 0.005 per diode per second, a factor of two better than the value required for H.R.S. science. The H.R.S. detectors have a dynamic range of *ca.* 2×10^7. The quantum efficiencies (q.e.) of the detectors selected for flight have also been measured. For the MgF_2–CsTe Digicon, the peak q.e., near 2537 Å, is 15.2%. A q.e. of 10.8% was measured for the LiF–CsI detector at 1216 Å. Both detectors are excellent with regard to measured distortion, photocathode uniformity, and number of blemishes and in-operable diodes. Such factors are of particular importance given the emphasis on photometric accuracy in the scientific programme of the H.R.S.

The wavelengths of astronomical spectral features in the ultraviolet have never before been measured to the accuracy that the H.R.S. will be capable of. Astronomical sources will therefore be insufficient as wavelength standards until the H.R.S. itself has been used to calibrate their spectra. For this reason, redundant, hollow-cathode Pt–Ne lamps are included in the H.R.S. design as internal wavelength references.

The builders of the H.R.S. have encountered the limits of current technology in several areas. Groove frequencies for the first-order gratings as high as 6000 mm^{-1} were required to achieve the desired resolution, $R > 1.8 \times 10^4$, over the entire wavelength range of the instrument. Such gratings were made successfully by two different manufacturers, using holographic techniques. Their measured peak efficiencies range from 25% for the 6000 mm^{-1} grating up to 65% for the 3600 mm^{-1} grating. Ruling of the concave cross-dispersers was also difficult because of the very shallow blaze angle (less than 1°) required. Each cross-disperser was ruled as a multi-partite grating to prevent undercutting by the ruling diamond. The H.R.S. design required an échelle grating with a large ruled area, high groove frequency, large blaze angle, high efficiency and minimum ghosts and scattered light. The parameters for the échelle, which were originally selected to provide optimum resolution and order separation, required a ruling that was expected to be well within the capabilities of current technology – more difficult échelles have been ruled in the past. Unfortunately, numerous attempts to rule the originally prescribed grating were unsuccessful. A substitute, commercially available échelle grating has now been selected. Its use will result in a small, acceptable loss in spectral resolution and order separation.

The Digicons used in both the H.R.S. and the F.O.S. represent advancements in detector technology. Digicons of smaller format have been in use at ground-based observatories for nearly a decade. For S.T. applications these devices were enlarged from 212 to 512 channels, requiring the development of a high-density header for vacuum-tight connections to the 512 independent electrical channels. Photocathode–window combinations appropriate for space astronomy were also incorporated in these Digicons for the first time.

The greatest technical challenge to the development of the H.R.S. has been in the construction of its hybrid electronics packages. The preamplifier and postamplifier hybrids are the

largest ever made for space flight. They are designed to minimize system noise and magnetic interference with the deflexion and focusing of the Digicon electron beams. After numerous difficulties, nearly all of the flight preamplifier hybrids have now been manufactured and production of the postamplifier packages is well under way.

At present most of the flight components of the H.R.S. have been made, subsystems testing is well advanced, and construction of the instrument is proceeding. Both the H.R.S. and the F.O.S. are scheduled to be delivered to the N.A.S.A. early in 1983.
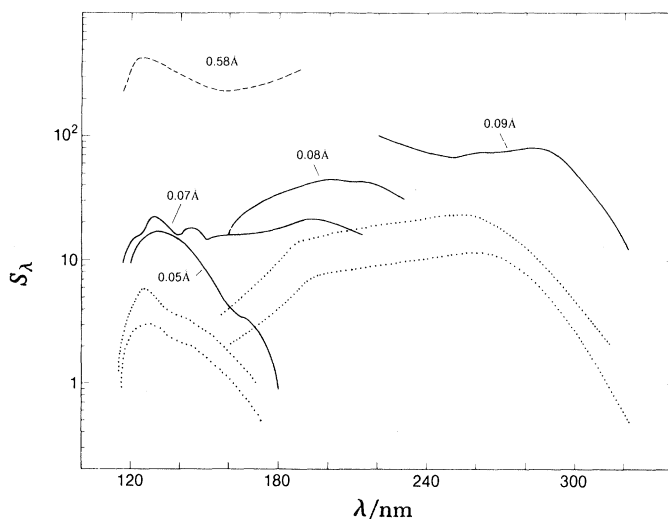

FIGURE 6. Composite sensitivity curves for the Space Telescope and High-Resolution Spectrograph. Spectroscopic modes with resolving powers $R \approx 2 \times 10^3$, 2×10^4 and 10^5 are denoted, respectively, by broken, solid and dotted curves. The two sets of curves for $R \approx 10^5$ are envelopes connecting the sensitivity maxima and minima within the 34 échelle orders. Approximate widths of resolution elements are labelled on the curves for first-order modes. Resolving power varies only weakly with wavelength in the échelle mode. The 0.25" aperture is assumed.

It is now possible, by using test data for flight components, to predict realistically the sensitivity of the H.R.S. and telescope system. This is illustrated in figure 6. Note that the curves for the highest-resolution mode are based on theoretical estimates of efficiency of the échelle grating, because measurements of the substitute échelle have not yet been completed.

The H.R.S. will have important applications to a broad range of astrophysical problems. It will be used in studies of the interstellar medium in our own galaxy and in neighbouring galaxies, in studies of stellar winds and other forms of stellar mass loss, and in studies of the chromospheres and coronae of stars. It will expand knowledge of the abundances of the chemical elements and of their relation to stellar and galactic evolution. The H.R.S. is sufficiently sensitive and noise-free to provide important observations of the brighter quasars and the bright, eruptive nuclei of active galaxies. It will also have numerous applications in the study of the atmospheres of objects in the Solar System: comets, planets and satellites.

An example of the vast improvement over previous spectroscopic capabilities in space that the H.R.S. will provide is illustrated in figure 7. Figure 7a shows a theoretical computation of a dense pattern of absorption lines, characteristic of that produced in the atmosphere of a sharp-lined, chemically peculiar, early-type star. In figure 7b this theoretical spectrum has been degraded to the resolving power of the *IUE* spectrograph, and clearly much of the original

spectral information is lost. Figure 7c illustrates the same spectrum as it should appear when observed with the highest-resolution mode of the H.R.S. It may even be possible to recover the minor amount of spectral information lost at this resolution with deconvolution techniques that take advantage of the H.R.S.'s stability and low background noise. In figure 8 are shown the expected 'limiting magnitudes' for a variety of normal and chemically peculiar stars in the effective temperature range 7500–17 000 K, at which one should achieve signal:noise ratios of *ca.* 20 in a 3 h integration at a wavelength near 1360 Å. These computations assume an average
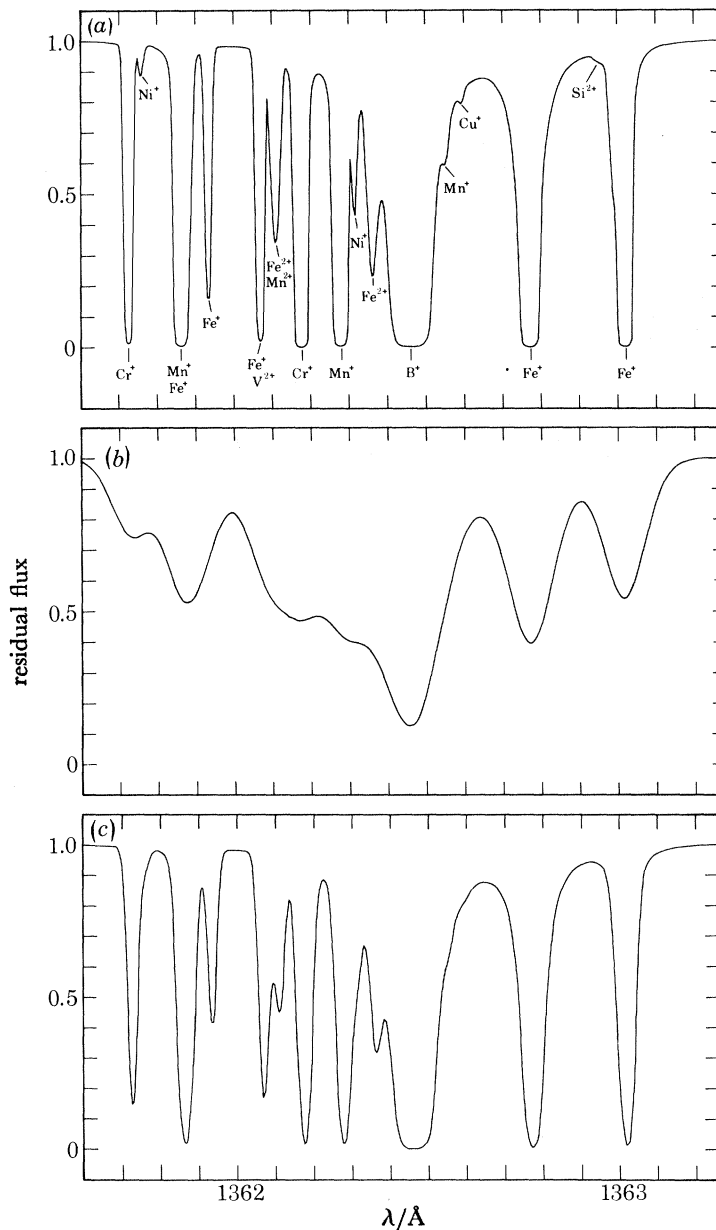

FIGURE 7. (a) Theoretical ultraviolet spectrum for a sharp-lined, chemically peculiar star, undegraded by instrumental broadening ($\lambda/\Delta\lambda = \infty$). (b) Same spectrum convoluted with the instrumental broadening function of the *International Ultraviolet Explorer* ($\lambda/\Delta\lambda = 1.2 \times 10^4$). (c) Same spectrum convoluted with the expected instrumental broadening of the High-Resolution Spectrograph ($\lambda/\Delta\lambda = 10^5$; $V \sin i = 3$).

interstellar extinction of 0.8 visual magnitudes per kiloparsec. In fact much less extinction will be found along many lines of sight through the patchy interstellar dust, fortuitously allowing observations of even fainter stars. The combined H.R.S.–S.T. system will clearly allow data of good quality to be obtained on objects that could barely be detected with the *IUE* and that could not be observed at all with *Copernicus*.

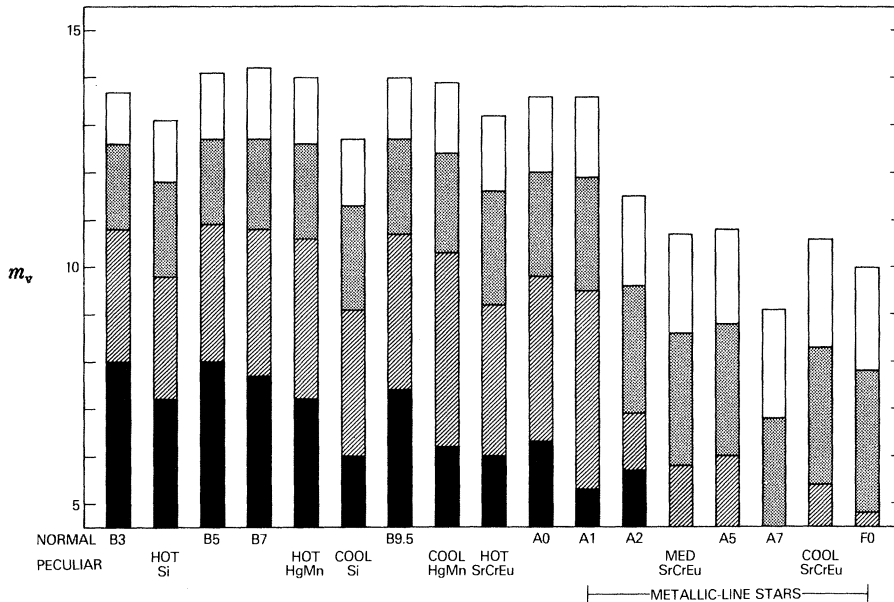Additional information about the H.R.S. may be found in Brandt *et al.* (1979, 1981).

FIGURE 8. Apparent visual magnitudes at *ca.* 1360 Å of normal and peculiar B and A-type stars that can be observed in the various modes of the H.R.S. and also with the *IUE* with a signal:noise ratio of *ca.* 20 in 3 h in the presence of 0.8 magnitudes per kiloparsec average visual extinction. H.R.S.: unshaded, $R \approx 2 \times 10^3$; stippled, $R \approx 2 \times 10^4$; hatched, $R \approx 10^5$. *IUE:* solid black, $R \approx 10^4$.

4. ADDITIONAL SPECTROSCOPIC CAPABILITIES

The $f/48$ optical train of the Faint Object Camera (F.O.C.) can be adapted for use as a long-slit spectrograph. The entrance aperture, located in the S.T. $f/24$ focal surface, is a slit with dimensions $0.1'' \times 20''$, projected on the sky. Upon command a convex relay mirror can be moved into the $f/48$ camera beam, deflecting it to a fixed plane grating. The spectrally dispersed stigmatic image of a $20''$ segment of the sky, spatially resolved perpendicular to the dispersion, is focused onto the detector photocathode. The resolving power is 2300. Overlapping first-order, second-order and third-order spectra are isolated with appropriate filters. These spectra cover respectively 3600–5400 Å, 1800–2700 Å and 1200–1800 Å. To orient the slit on the sky, one must roll the entire S.T., a procedure that is limited by spacecraft operational constraints. Over a period of several months, however, any desired position angle may be obtained. The long-slit spectrograph is less efficient than the F.O.S. described in §2 by about a factor of three at 3600 Å, when allowances are made for differences in resolution and slit width. However, it provides a unique capability for the study of extended sources – galaxies, clusters and nebulae – in programmes requiring both spatial and spectral information. Examples include the determination of the velocity dispersions in nuclei of galaxies and globular

clusters, measurement of the variation of metal content with radius in globular clusters and elliptical galaxies, and determination of the temperature and density distributions in nebulae and supernova remnants.

Both S.T. cameras incorporate 'objective prism' spectroscopic modes, i.e. the capability to disperse spectrally all of the images in their fields of view simultaneously, with low resolving power. Both the $f/48$ and $f/96$ optical trains of the F.O.C. contain two prisms mounted in their filter wheels. One of these, a single prism made of MgF_2, covers the bandpass from 1200 to 7000 Å with resolving power of *ca.* 50 in both relays. The other, a double prism of MgF_2 and silica, operates from 2000 to 7000 Å. At $f/96$, its resolving power is *ca.* 100; at $f/48$, $R \approx 50$. The Wide-Field and Planetary Camera's filter wheels contain three 'grisms', i.e. transmission gratings ruled on prism substrates. Two of the 'grisms' provide first-order spectra, one of which extends from 3300 to 6400 Å, the other from 5700 to 12000 Å. Their substrates filter the higher orders. For low-resolution ultraviolet spectroscopy a 'grism échelle' has been designed for the W.F.P.C. In this case the ruled area is on a CaF_2 substrate possessing two wedge angles, permitting the separation of first-order and second-order spectra in the cross-dispersion direction. The blaze wavelengths are near 2400 Å in first order and near 1560 Å in second order. Narrow-band filters can be introduced into the beam to block out either order if necessary to minimize field confusion. The dispersion of the W.F.P.C. 'objective grisms' is about 60 Å per pixel in first order. Using these devices in the F.O.C. and in the W.F.P.C., observers will systematically search entire fields of view for objects of a particular class, e.g. faint quasars, optical counterparts of X-ray sources. From such images, information may immediately be derived about the flux distributions and red shifts of these objects. Further details about the F.O.C. may be found in Macchetto *et al.* (1980).

References

Allen, R. G. & Angel, J. R. P. 1982 *Proc. Soc. photo-opt. Instrumn Engrs* **331**. (In the press.)
Bahcall, J. N. & O'Dell, C. R. 1980 In *Scientific research with the Space Telescope* (*IAU Colloquium* no. 54) (NASA CP-2111), p. 5.
Brandt, J. C. *et al.* 1979 *Proc. Soc. photo-opt. Instrumn Engrs* **172**, 254.
Brandt, J. C. *et al.* 1981 *Proc. Soc. photo-opt. Instrumn Engrs* **279**, 183.
Harms, R. J. *et al.* 1979 *Proc. Soc. photo-opt. Instrumn Engrs* **183**, 74.
Harms, R. J. *et al.* 1982 *Proc. Soc. photo-opt. Instrumn Engrs* **331**. (In the press.)
Leckrone, D. S. 1980 *Pub. astron. Soc. Pacif.* **92**, 5.
Macchetto, F., van de Hulst, H. D., Alighieri, A. & Perryman, M. A. C. 1980 ESA SP-1028.

Discussion

J. P. CONNERADE (*Imperial College, London, U.K.*). Dr Leckrone mentioned the probable use of a 6000 lines nm^{-1} holographic grating in the Space Telescope. It may be of interest that we have experienced a strong dependence of the efficiency of such gratings on the polarization of incident light. This was found in studies with synchrotron radiation and has been attributed to the large angle at which high-density rulings are used in 'normal incidence' mounts. I would suggest that it may be possible to obtain information on the polarization of celestial objects if the telescope can be rotated.
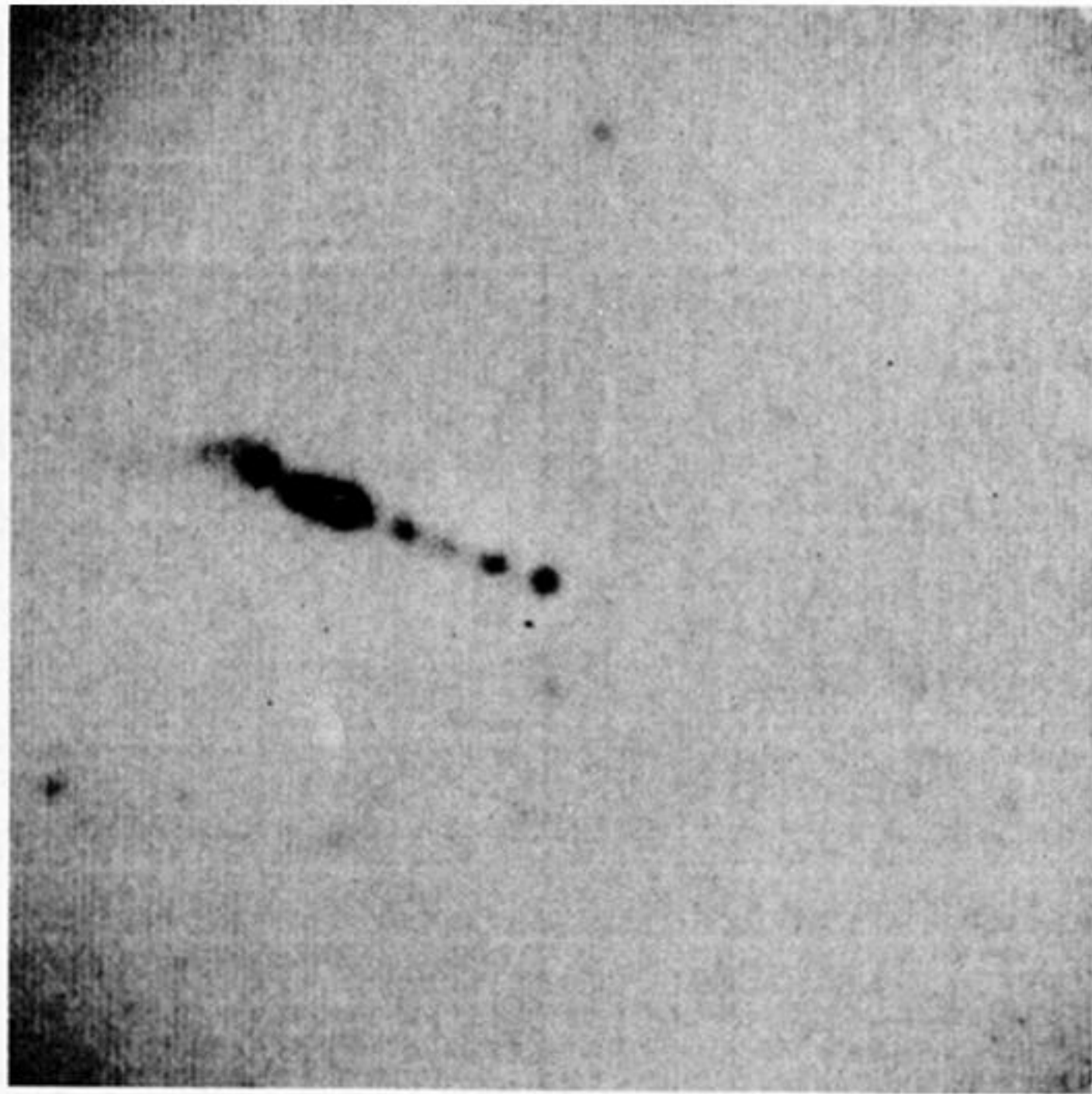
[95]

FIGURE 3. Image of the radio galaxy M87, processed to highlight the nucleus and jet. Photo courtesy of J. A. Westphal, California Institute of Technology.